EAI Endorsed Transactions
on Energy Web
Research Article EAI.EU

Comparative study on the accuracy and robustness of piezoelectric valve flow prediction models based on deep learning

Yafei Zhong[1,2,3], Xudong Wang[1,2,3,*], Tao Wang[4], Zhen Zhang[1,2,3], Heran Hu[1,2,3], Kunyi Wan[4], Lina Wang[4], Lei Shi[4]

[1]Beijing Institute of Control Engineering, Beijing, China
[2]Advanced Space Propulsion Technology Laboratory, Beijing, China
[3]Beijing Engineering Research Center of High-Efficiency & Green Aerospace Propulsion Technology, Beijing, China
[4]Tianjin University, Tianjin, China

Abstract

To enhance the dependability and autonomy of the μg/s piezoelectric flow control device in long-term on-orbit operations, the on-orbit adaptability and robustness of various deep learning prediction models are compared and analyzed. Multidimensional time series data such as excitation voltage, spool displacement, inlet pressure, and valve body temperature were acquired and normalized. The accuracy of flow prediction was assessed using three models: standard Long Short-Term Memory (Standard LSTM) network, Attention LSTM, and convolutional neural network LSTM (CNN-LSTM). The models' robustness was evaluated using several sensor degradation scenarios. CNN-LSTM has the best flow prediction ability. Compared with the Standard LSTM, the CNN-LSTM reduces absolute error (MAE) by 34.59 μg/s and relative error (MRE) by 2.82% when four-dimensional parameters are supplied (baseline state). The displacement of the valve spool is the key characteristic. When provided with a unit displacement signal, both Attention-LSTM and CNN-LSTM exhibit excellent flow prediction capabilities. The prediction error of the three LSTM models increases significantly when this feature is removed. Following the removal of the displacement feature using the CNN-LSTM model, the MRE and MAE exceed the baseline by 69.65% and 406.55 μg/s, respectively. Furthermore, the CNN-LSTM model demonstrates superior robustness in the scenario of forward-filled missing data, whereas the Attention-LSTM exhibits outstanding robustness in the presence of random noise. However, when confronted with sensitivity deterioration and signal drift, the prediction accuracy and robustness of all three models experience a significant decline.

Keywords: piezoelectric valve, μg/s flow control, deep learning, model robustness, CNN-LSTM

Received on 21 July 2026, accepted on 19 August 2026, published on 21 September 2026

doi: 10.4108/ew.14119

1. Introduction

Space gravitational wave detection is a frontier field for verifying general relativity and exploring the secrets of the cosmos, which requires exceptionally high spacecraft stability [1-2]. Driven by this scientific goal, the next generation of drag-free satellites must be equipped with ultra-quiet and ultra-high-precision propulsion systems that can precisely compensate for residual atmospheric drag and solar-radiation pressure. As a result, research has focused on continuously adjustable micro-newton propulsion technology. To establish an almost ideal experimental environment for scientific loads, the thrust output must not only have high resolution and low noise characteristics, but also be capable of continuous throttling over a wide operating range [3-4].

*Corresponding author. Email: kyffwd@163.com

Among the available micro-Newton propulsion technologies, the flow control technology based on a piezoelectric ceramic drive offers distinct advantages because of its nanoscale displacement resolution [5-7]. The flow of the piezoelectric valve directly influences the propulsion system's thrust output performance, therefore, accurate flow measurement and control are critical. Scholars have conducted extensive research on the intrinsic hysteresis, creep, and nonlinear properties of piezoelectric materials. Yu et al. developed a mathematical model to correct for the piezoelectric actuator's hysteresis nonlinearity [8]. Gu et al. conducted a systematic evaluation of the modeling and control methodologies used in piezoelectric drive positioning platforms, highlighting the significant challenge of achieving high-precision control due to complicated nonlinear interference [9]. However, traditional control approaches frequently rely on complicated mathematical analytical models. Under multiphysics coupling conditions, parameter identification is challenging, and real-time performance is difficult to ensure.

Furthermore, to fulfill the criteria of spacecraft test coverage, flow calibration under coupled multi-parameter conditions is labor-intensive, making it difficult to meet engineering-scale production and calibration requirements in engineering practice. Deep learning technology introduces a new approach to handling nonlinear prediction issues. The long short-term memory (LSTM) network was first proposed by Sepp Hochreiter and Jürgen Schmidhuber in 1997 and innovatively introduced a "cell state" and gating mechanisms in order to fundamentally solve the vanishing-gradient problem inherent in traditional RNN when processing long sequences [10]. LSTM's gating mechanism makes it highly effective for time series processing, with successful applications across various industries [11-18]. In recent years, scientists have developed a variety of advanced architectures and attempted to apply them to piezoelectric systems: Liu et al. showed that LSTM can effectively capture the dynamic properties of piezoelectric ceramics, including creep and hysteresis, demonstrating that LSTM's temporal memory mechanism is well-suited to the historical dependence characteristics of piezoelectric valve flow [19]. Patil et al. used an LSTM network to determine the displacement of a piezoelectric actuator, proving that the model accurately mimics the actuator's hysteresis behaviour [20]. Baker et al. employed an LSTM-based estimator to create a data-driven, self-calibrating intelligent model for a piezoelectric valve that projected downstream pressure and addressed flow control drift [21].

According to the previously mentioned literature, it is challenging to determine the correct mapping relationship between flow rate and other dynamic parameters of piezoelectric systems because of the nonlinear errors caused by the intrinsic hysteresis and creep of piezoelectric materials; LSTM architectures offer significant advantages in capturing the dynamic properties. Identifying the parameters that most significantly impact flow prediction accuracy is crucial for the redundant design of sensors. Furthermore, during long-term on-orbit spacecraft operations, sensor aging and temperature variations result in data missing, random noise, signal drift, and sensitivity deterioration. However, little research has investigated the robustness of LSTM models under signal distortion. Therefore, distinct from studies focusing solely on theoretical accuracy, the primary novelty of this work lies in a comprehensive robustness evaluation under sensor degradation scenarios: specifically missing data, random noise, sensitivity deterioration, and signal drift. To address these challenges, the study makes the following contributions: (1) developing a multiparameter data-driven LSTM model for flow prediction; (2) comparing the predictive accuracy of three flow prediction models (Standard LSTM, Attention-LSTM, and CNN-LSTM) and suggesting the optimal prediction approach. (3) quantitatively validating the model's robustness against the aforementioned realistic fault conditions.

This paper establishes an important theoretical foundation for intelligent health management and control strategy optimization in high-reliability spacecraft propulsion systems.

2. Experimental scheme and neural network model

2.1 Experimental scheme

In this study, an experimental apparatus for testing microflow characteristics is specifically designed and manufactured. As shown in Figure 1(a), the platform consists of four main subsystems: a pressure control unit, a flow measurement unit, a spool displacement measurement unit, and a temperature measurement unit. The pressure control unit employs an Alicat PC-100PSIA-D-PCV high-precision electronic pressure regulator. The equipment uses an innovative closed-loop control method to provide stable pressure output over the region of 0.1-0.3 MPa. To ensure pressure stability, a 0.75 L buffer tank is added at the end of the pipeline. This design ensures that system pressure fluctuations are maintained within a 0.5% error band, thereby eliminating the interference of upstream pressure pulsation on test results.

A high-precision thermal mass flowmeter with a full-scale range of 200 SCCM was selected to accommodate the low-pressure and microflow operating conditions of the piezoelectric valve. Prior to experimentation, the mass flowmeter was calibrated using a micro-gas standard device. The calibrated measurement uncertainty is 1% of Full Scale (FS), ensuring the reliability of the data acquisition, and a dynamic response time of less than 10 ms, meeting the system's requirements for capturing transient characteristics.

Nitrogen (N2) was employed as the working gas. The conversion from volumetric flow (SCCM) to mass flow rate (μg/s) is based on standard reference conditions of 298.15 K and 101.325 kPa. The relationship is defined by the equation: Mass Flow Rate(μg/s) = 19.08 × Volumetric Flow Rate (SCCM).

Accurate measurement of spool displacement is essential in this study. In the experiment, a high-precision capacitive displacement sensor is employed to measure the spool displacement in real time. The sensor is installed with one end fixed to the valve spool and the other end fixed to the base. It has a wide range of 0.002-100μm with a resolution of better than 1 nm. Its nonlinearity is within ±1% of full scale.

The temperature control unit consists of a temperature-controlled test chamber and a distributed temperature-monitoring network. The test chamber simulates temperatures from -20°C to 100°C with an accuracy of ±0.1 °C. The valve body's temperature is monitored in real time using a thermistor with an accuracy of ±0.1 °C.

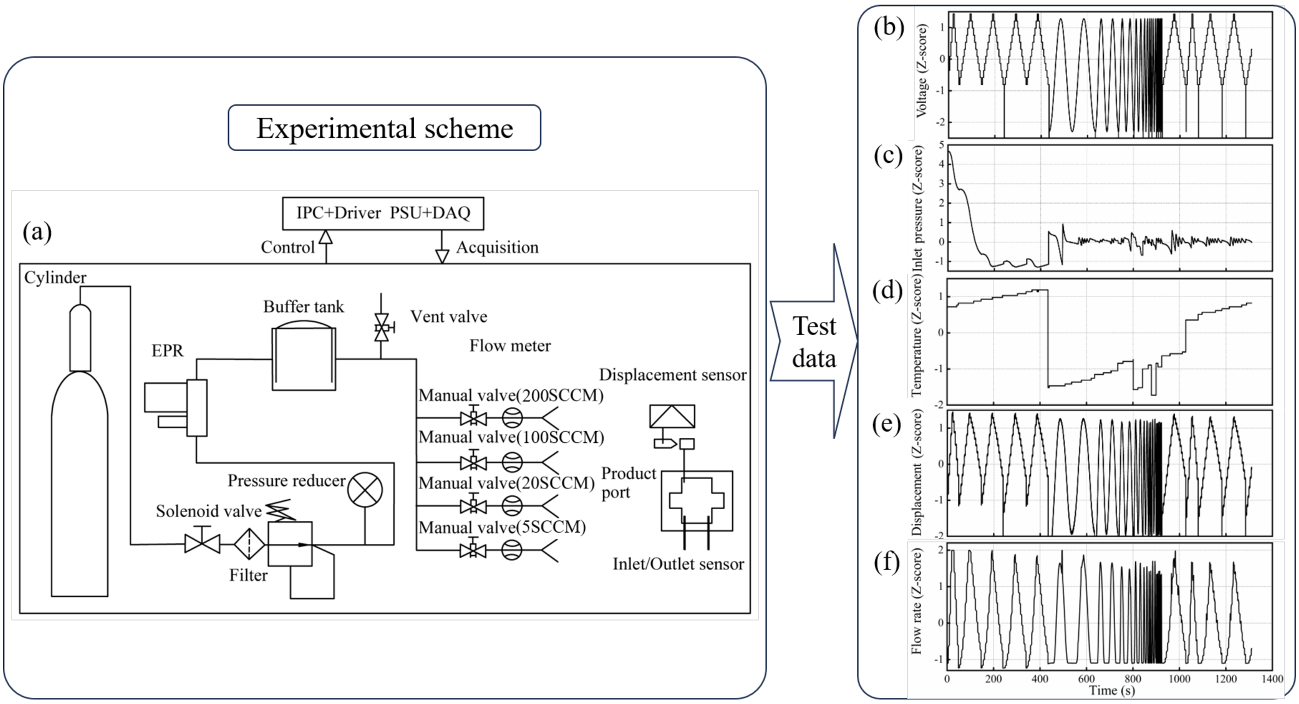

Figure 1. Experimental advanced deep learning model: (a) Experimental scheme ; (b) Excitation voltage ; (c) Inlet pressure ; (d) Valve body temperature ; (e) spool displacement ; and (f) output flow rate

The experimental procedure involves setting the system's initial pressure to 0.15 MPa, the temperature of the test chamber to 25 °C, and applying a periodic square wave voltage excitation signal to the piezoelectric valve. Simultaneously, the displacement closed-loop control approach is employed to progressively adjust the valve port opening from 1% to 99% of the full opening. All sensor data is collected synchronously at a sampling frequency of 50 Hz, yielding a time series of 70,000 synchronized sampling points. These data cover various operating states of the piezoelectric valve and provide adequate data support for training and verifying the subsequent deep learning model. The parameters gathered include physical variables such as the control voltage, inlet pressure, valve body temperature, spool displacement, and output flow. As illustrated in Figure 1, before model training, all input and output variables were standardized using Z-score normalization (i.e., removing the mean and dividing by the standard deviation) to avoid the potential impact of varying physical dimensions on the model training process.

2.2 Training method

The model utilizes a multidimensional input space comprising excitation voltage, inlet pressure, valve-body temperature, and spool displacement to predict the piezoelectric-valve flow rate, thereby establishing a nonlinear multiple-input, single-output mapping, as illustrated in Figure 2. To strictly prevent look-ahead bias, the dataset was partitioned chronologically without random shuffling. Specifically, the data were split into training and testing sets at a ratio of 7:3. The first 70% of the time-series data served as the training set for parameter learning, while the remaining 30% were reserved as a hold-out test set to evaluate generalization on unseen future data.

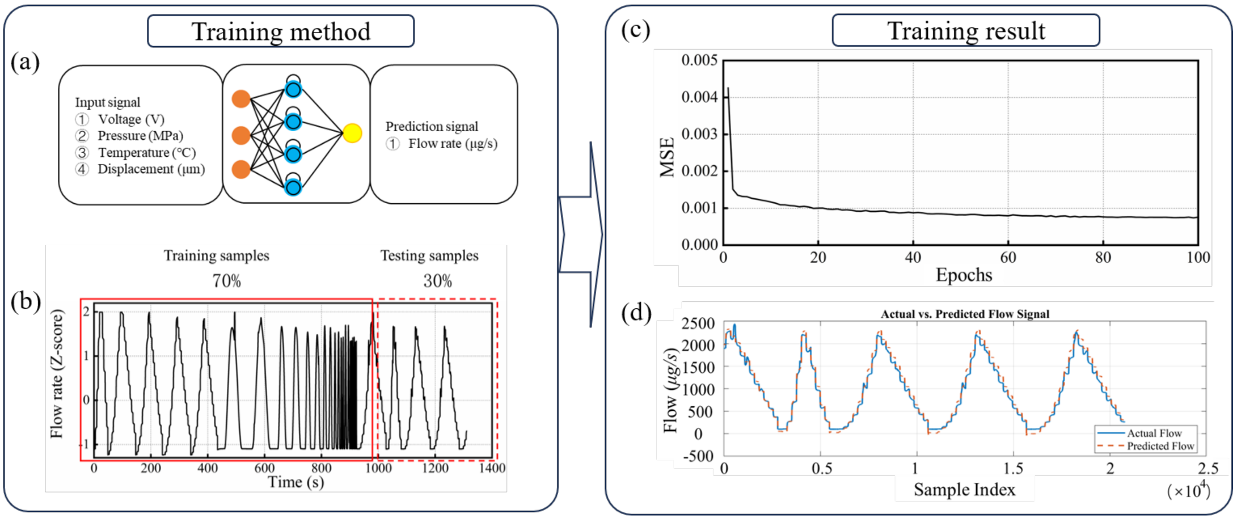

Figure 2. Training methods and training results (a) Training model ; (b) Data splitting method; (c) Mean squared error distribution; and (d) Training results

The hyperparameters for all compared models were explicitly defined to ensure a fair comparison. The Standard LSTM, Attention-LSTM, and CNN-LSTM models were constructed with 2 layers, and a dropout rate of 0.2 was applied to them to prevent overfitting. All models were trained using the Adam optimizer with a learning rate of 0.005, and the Mean Squared Error (MSE) was employed as the loss function, as illustrated in Figure 2 (c). Regarding the training configuration, the mini-batch size was set to 12 to balance training efficiency with parameter update stability. The maximum number of epochs was set to 100, which was determined through internal validation on the training set to ensure convergence without overfitting. Furthermore, to rigorously validate robustness under varying data integrity conditions, sensor degradations were simulated with data missing rates of 10% and 30%.

To evaluate the prediction accuracy and generalization capacity of the models, the Mean Absolute Error (MAE) and Mean Relative Error (MRE) are utilized as the primary evaluation metrics. MAE and MRE are calculated on the inverse-transformed test sets to accurately reflect real-world physical values. Since the output flow of the piezoelectric valve may contain low-flow or near-zero-flow regions, the calculation of the relative error can be highly sensitive to the denominator, potentially leading to numerical instability. To avoid this issue when the actual flow approaches zero, the standard practice of introducing a small constant ε into the denominator is adopted. The formulas for MAE and MRE are defined as:

$$MAE = \frac{1}{N}\sum_{i=1}^{N}|y_i - \widehat{y_i}| \tag{1}$$

$$MRE = \frac{1}{N}\sum_{i=1}^{N}\frac{|y_i-\widehat{y_i}|}{|\widehat{y_i}|+\varepsilon} \tag{2}$$

Where N represents the total number of test samples, y_i is the actual measured flow value at the i-th sample, and $\widehat{y_i}$ denotes the corresponding predicted value, ε is a small constant (e.g., 10^{-6}).

2.3 Neural network construction

The purpose of this work is to assess the performance of several deep learning architectures on the piezoelectric valve flow prediction challenge. To this end, three LSTM-based models are developed and implemented: Standard LSTM, Attention-LSTM, and CNN-LSTM. The model architectures are detailed as follows:

Standard LSTM

In this study, Standard LSTM and two LSTM-based variants were constructed. The Standard LSTM unit regulates the update of the cell state Ct and the output of the hidden state ht through the input gate it, forget gate ft and the output gate ot. The core state transition equations are as follows:

$$f_t = \sigma(W_f \cdot [h_{t-1}, x_t] + b_f) \tag{3}$$

$$i_t = \sigma(W_i \cdot [h_{t-1}, x_t] + b_i) \tag{4}$$

$$\widetilde{C_t} = tanh(W_C \cdot [h_{t-1}, x_t] + b_C) \tag{5}$$

$$o_t = \sigma(W_o \cdot [h_{t-1}, x_t] + b_o) \tag{6}$$

$$C_t = f_t \circ C_{t-1} + i_t \circ \widetilde{C_t} \tag{7}$$

$$h_t = o_t \circ tanh(C_t) \tag{8}$$

Where h_t represents the hidden state at time t, σ is the sigmoid activation function, W_f, W_i, W_C, W_o are weight matrices, b_f, b_i, b_C, b_o are the bias terms, $\circ$ represents element-by-element multiplication (Hadamard product), C_t is the current cell state. Based on this standard architecture, two variants were further constructed.

Attention-LSTM

The Attention-LSTM mechanism is introduced to mitigate the loss of relevant information over long input sequences. The model generates the context vector c_t and determines the weight α_i based on the correlation between the hidden state h_T at time step T and the historical state h_i.

$$e_i = v^T tanh(W_h h_i + W_s h_T + b) \quad (9)$$

$$\alpha_i = \frac{\exp(e_i)}{\sum_{k=1}^{T} \exp(e_k)} \quad (10)$$

$$c_t = \sum^T \alpha_i \, h_i \quad (11)$$

To improve the model's capacity to capture important signal variations, the context vector c_t and the current state h_T determine the final prediction output.

CNN-LSTM

CNN-LSTM employs a serial coupling structure, extracts local temporal patterns using a one-dimensional convolutional network, and then feeds this information into the LSTM layer to capture temporal relationships. The convolutional layer extracts features from the input sequence (X), yielding the output feature map Fk of the k-th convolution kernel as follows::

$$F_k = ReLU(W_k * X + b_k) \quad (12)$$

The LSTM network receives the following feature sequence Z after max pooling:

$$Y_{pred} = Dense(LSTM(Z)) \quad (13)$$

3. Results and Discussion

3.1 Comparison of prediction ability of different LSTM models

This section includes five sets of comparative experiments meant to investigate the impact of varied input parameters and LSTM models on flow forecast accuracy. Table 1 summarizes the performance of the three models under each input-feature configuration, with P, T, D, and V representing pressure, temperature, displacement, and voltage, respectively (for example, Case_D denotes a model using displacement as the sole input feature).

Table 1. Performance comparison of different neural network models

Experimental group	Attention-LSTM		CNN-LSTM		Standard LSTM	
	MAE(μg/s)	MRE(%)	MAE(μg/s)	MRE(%)	MAE(μg/s)	MRE(%)
Case_PTDV	71.52	11.53	44.24	8.50	78.83	11.32
Case_D	86.13	7.48	50.34	5.99	88.83	15.83
Case_V	251.73	50.41	264.56	48.29	245.17	75.97
Case_PTD	44.11	9.85	124.54	14.33	47.51	8.12
Case_PTV	273.66	68.89	450.79	78.15	494.64	191.16

Notes: P-Pressure, T-temperature, D-Displacement, V-Voltage

The experimental results demonstrate that the displacement feature is critical in the flow prediction task. It had a substantial effect in both the feature-removal and single-feature experiments. When the displacement characteristics were removed from the benchmark combination comprising all four features, the prediction performance of all models deteriorated substantially. For Attention-LSTM, the mean absolute error (MAE) increased from 71.52 to 273.66, while the relative error (MRE) climbed from 11.5% to 68.9%. The MAE of CNN-LSTM surged from 44.24 to 450.79. This indicates that pressure, temperature, and voltage features cannot replace the critical information included in displacement characteristics.

This result can be explained by the relationships between the four input variables and the flow rate. Table 2 summarizes the correlations between pressure, temperature, voltage, displacement, and flow rate. The flow rate was strongly correlated with voltage and displacement, with correlation coefficients of 0.834 and 0.899, respectively. Figure 3 illustrates a heat map of voltage and displacement versus flow rate. The high-density region near a flow rate of -1 indicates that the system has a beginning threshold, and the displacement reaction to flow rate change is more sensitive than voltage. When the threshold is reached, the flow rate rises linearly with the increase of the independent variable. Because of the hysteresis effect [22], the high-density region in Figure 3 (a) is more dispersed than that in Figure 3(b), showing that flow rate is not reproducible under the same voltage. In contrast, the relationship between displacement and flow rate is unique, which is the primary cause of the decline in prediction accuracy once the displacement variable is eliminated.

Table 2. Correlation between four parameters and flow rate

Correlation	Pressure	Temperature	Voltage	Displacement
Flow rate	0.002	0.122	0.834	0.899

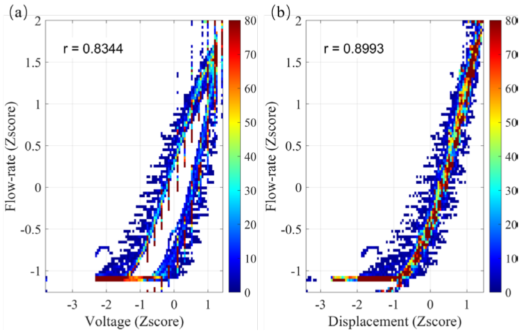

Figure 3. Parameter heat map (a) voltage vs flow rate (b) displacement vs flow rate

Figure 4 depicts the time histories of the predicted signal with the Attention-LSTM and CNN-LSTM. As demonstrated in Figure 4 (a), even when only the displacement signal is used as an input (Case _ D), the model's prediction curve remains close to the real value, indicating a good fitting effect in most time periods. Noticeable prediction errors occur mainly near several troughs of the flow signal. Typically, the relative error is within 10% and the absolute error is less than 100μg/s. These results demonstrate that the displacement signal is a highly informative predictor in flow prediction.

In the situation of missing displacement signal input, the model prediction curve deviates significantly from the true values. Specifically, the CNN-LSTM model systematically overestimates the flow during both the rising and falling phases. Furthermore, it introduces abnormal high-frequency fluctuations into the output. This suggests that the CNN module is overly sensitive to local deviations in the remaining input features, causing high-frequency oscillations in the predictions. Consequently, the model captures only the overall trend and fails to accurately reproduce the actual dynamics. In contrast, the Attention-LSTM provides a superior prediction of the decay trend. This improvement is attributed to the attention mechanism, which dynamically allocates weights to automatically focus on the key features that most significantly impact the prediction.

Unlike the displacement feature, the effect of the voltage feature is model-dependent. The performance of multiple models improves upon removing voltage from the input feature set. Nevertheless, the voltage reduction has minimal effect on the transient prediction deviation. For example, after removing the voltage feature, the MAE values of the Attention-LSTM and Standard LSTM models dropped from 71.52 and 78.83 to 44.11 and 47.51, respectively. The performance improvement after removing the voltage signal can be attributed to the physical mechanism of the piezoelectric actuator. A nonlinear hysteresis loop characterizes the relationship between the excitation voltage and the flow rate, as seen in Figure 3 (a). Incorporating voltage as a feature introduces severe nonlinear interference and noise, which hinders the LSTM model from accurately predicting the true flow rate. Since the relationship between spool displacement and flow rate is free from hysteresis, displacement serves as a direct and accurate physical state. When displacement is already utilized as an input feature, voltage becomes an indirect and redundant variable. Eliminating this redundant feature reduces model complexity and improves the fitting accuracy.

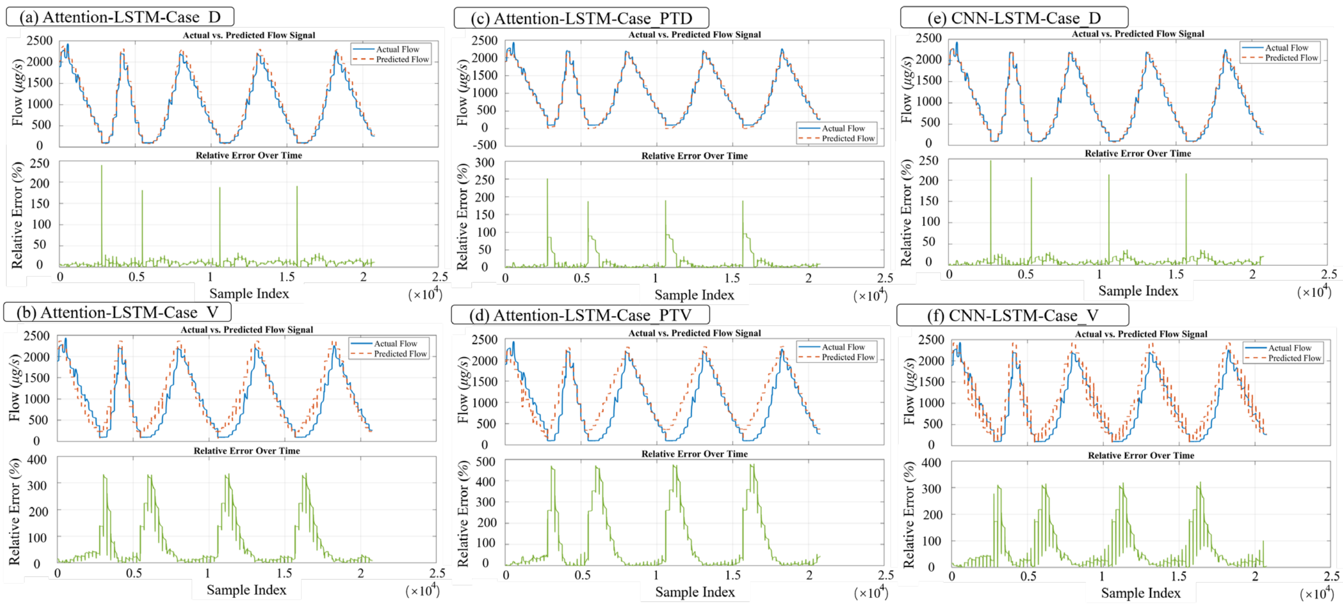

Figure 4. Timing diagram of the original and predicted signals：(a)Attention-LSTM, Case_D; (b)Attention-LSTM, Case_V; (c)Attention-LSTM, Case_PTD; (d)Attention-LSTM, Case_PTV; (e)CNN-LSTM, Case_D; and (f)CNN-LSTM, Case_V

Based on the preceding analysis, the following conclusions and recommendations are drawn: Regarding the input variables for flow prediction, essential features should be prioritized while interference factors are minimized. It is recommended to exclude voltage from the model deployment, as the combination of pressure, temperature, and displacement constitutes the optimal input set. Concurrently, ensuring the data quality and stability of the displacement sensor is critical. Furthermore, both Attention-LSTM and CNN-LSTM demonstrate superior performance in flow prediction when the quality of the core signals is high.

3.2 Model prediction performance under sensor signal degradation

This section comprehensively evaluates the prediction performance and robustness of three LSTM-based models under simulated sensor signal degradation scenarios. To assess the models' robustness, only the displacement sensor input was subjected to four degradation scenarios (random data missing and repair, random noise, sensitivity deterioration and signal drift), while the other input features remained unchanged. The mathematical formulations for these four scenarios are defined as follows: Random data missing is defined by a probability p, where data points are randomly dropped. The remaining scenarios are formulated in Equations (14)-(16).

$$S_{noise}[i] = s_i + \sigma(S) * L_n * \epsilon_i \tag{14}$$

$S_{noise}[i]$ denotes the i-th data point of the noisy signal, s_i represents the pristine signal. $\sigma(S)$ is the standard deviation of the pristine signal. Additionally, L_n is the noise intensity coefficient. ϵ_i is a random variable drawn from a standard normal distribution.

$$S_{sens}[i] = s_i * (1 - \frac{i-1}{N-1} * L_s) \tag{15}$$

$S_{sense}[i]$ is the i-th data point of the signal under the sensitivity drop condition. L_s represents the maximum decay ratio, N corresponds to the total number of test samples.

$$S_{drift}[i] = s_i + \frac{i-1}{N-1} * (S_{max} - S_{min}) * L_d \tag{16}$$

$S_{drift}[i]$ is the i-th data point of the drifted signal. S_{max} and S_{min} are the maximum and minimum values of the pristine signal, respectively. L_d is the drift ratio amounting to the peak-to-peak value.

It is crucial to note that all these mathematical disturbances were applied directly to the pristine data before the Z-score normalization process, ensuring a highly realistic simulation of actual sensor degradation behaviors in engineering environments. In this sensor degradation evaluation, the fault onset is strictly defined at the first time step of the test set, with the fault duration spanning the entire length of the test sequence. During the application phase, the model is trained exclusively on the pristine dataset, and all corruption scenarios are applied solely at test time. Furthermore, regardless of the degree of input degradation, the ground truth remains completely uncorrupted, ensuring that the evaluation metrics accurately reflect the model's prediction deviations from the true physical state.

Table 3 summarizes the baseline performance of the three models using all four input features, under pristine conditions. Since error metrics such as MAE or MRE cannot explicitly reveal the extent of prediction performance loss caused by sensor degradation, the degradation ratio (R_{deg}) is introduced to quantitatively evaluate model robustness. It is defined as follows:

$$R_{deg} = \frac{MAE_{\mathrm{d}} - MAE_c}{MAE_c} \tag{17}$$

Where: MAE_{d} represents the mean absolute error under degraded data conditions. MAE_{c} represents the mean absolute error under pristine data conditions.

Table 3. The performance of each LSTM model under baseline state

Model	MAE(μg/s)	MRE(%)
Attention-LSTM	71.52	11.53
CNN-LSTM	44.24	8.50
Standard LSTM	78.83	11.32

Random Data missing and repair

Figure 5 depicts the timing diagram for 30% displacement sensor data missing and repair. Table 4 displays the expected MAE of each model using forward filling for random missing rate of 10% and 30%, respectively.

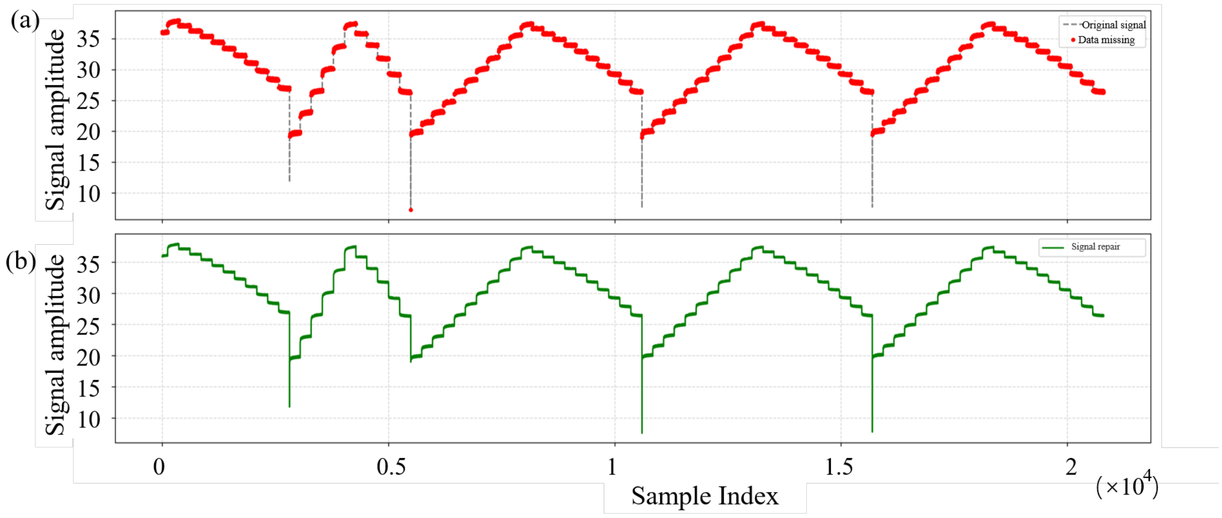

Figure 5. 30% displacement sensor data missing and forward filling (a) Timing diagram of 30% missing data; and (b) Timing diagram after forward filling

Table 4. Performance of each LSTM model in the case of random data missing

Model	Missing rate	MAE-Forward filling	R_{deg} (%)
Attention-LSTM	10%	71.53	0.01
Attention-LSTM	30%	71.5	-0.03
CNN-LSTM	10%	44.12	-0.27
CNN-LSTM	30%	43.81	-0.97
Standard LSTM	10%	78.86	0.04
Standard LSTM	30%	78.77	-0.08

As shown in Table 4, at random missing-data rates of 10% and 30%, the performance of all models remains remarkably stable following forward filling repair. Specifically, the MAE-Forward filling values for the CNN-LSTM model actually decrease from the baseline (44.24) to approximately 44.12 and 43.81, resulting in negative R_{deg} of -0.27% and -0.97%, respectively. Similarly, the Attention-LSTM and Standard LSTM models exhibit only minor fluctuations, with R_{deg} hovering near zero. In comparison, the CNN-LSTM model demonstrates the best robustness. These results indicate that when simple interpolation techniques are applied, these models possess strong robustness against local and discontinuous data missing. In practical applications, this implies that stable prediction performance can be maintained as long as data missing is detected in a timely manner and the traditional forward filling repair method is employed.

The effectiveness of forward filling stems from its fundamental assumption: the system's state at the previous time step is highly likely to be similar to the current state. Given that the state of the piezoelectric valve changes minimally over extremely short periods, its signal maintains a smooth, "step-like" morphology. Forward filling preserves the continuity of the input sequence, which is crucial for maintaining the stability of sequence models that rely on historical memory.

Random noise

Figure 6 depicts the displacement signal timing diagram for three signal degradation modes, as well as the CNN-LSTM flow-prediction results. Table 5 describes the performance of each prediction model under various signal degradation scenarios.

The Attention-LSTM model demonstrates superior robustness. Although its Mean Relative Error (MRE) hovers around 11.5%, which is comparable to that of the Standard LSTM, it exhibits the strongest resistance to intensifying data noise. As the noise level increases from 0.1 to 0.2, its MAE rises only marginally from 71.31 μg/s to 72 μg/s, resulting in a negligible R_{deg} of 0.67%. This indicates that the attention mechanism can effectively maintain prediction consistency even in the presence of data noise.

In contrast, the CNN-LSTM model exhibits the poorest robustness. While it achieves the lowest relative error (MRE=6.24%–6.68%) under pristine data conditions, its stability is severely compromised as the noise level increases. At a noise level of 0.2, it yields a drastic R_{deg} of 19.08%, the highest among all tested models. This suggests that despite its excellent fitting performance on clean data (low MRE), the CNN-LSTM lacks the adaptive capacity to handle sensor noise compared to the Attention-based approach. Fundamentally, this is because CNN rely on local convolutional kernels for feature extraction, making them highly susceptible to being misled by noise. Conversely, attention mechanisms inherently possess noise-resilient capabilities by dynamically focusing on critical information via global weights.

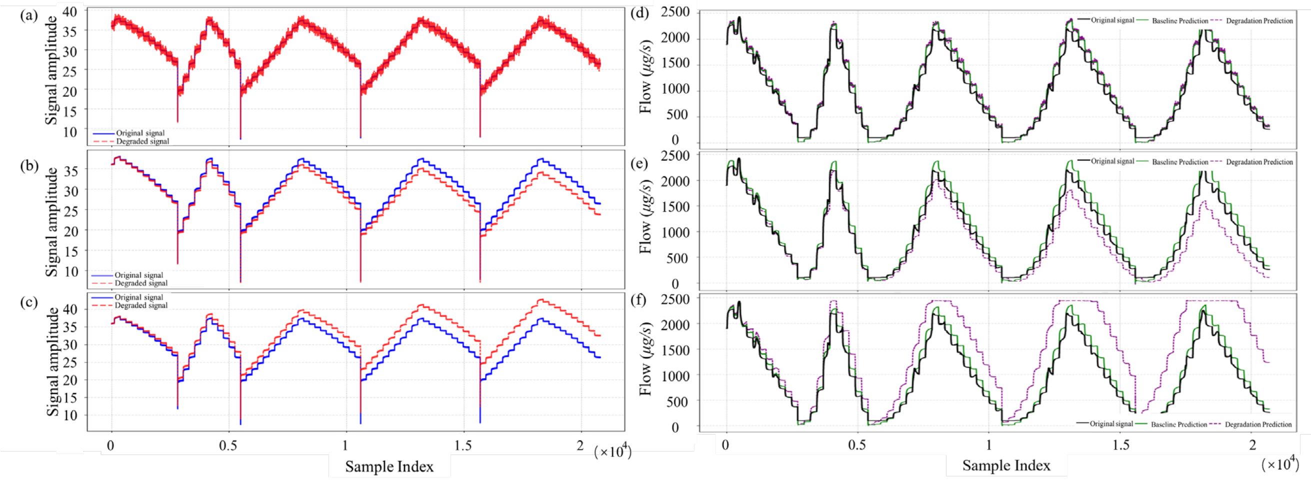

Figure 6. Timing diagram of displacement signal for degradation modes and CNN-LSTM prediction: (a) L_n =0.1, (b) L_s =0.1; (c) L_p =0.2; (d) Prediction with L_n =0.1, (e) Prediction with L_s =0.1; and (f) Prediction with L_p =0.2

Table 5. Performance comparison of different models under various degradation scenarios

Random noise	Model	Attention-LSTM-0.1	Attention-LSTM-0.2	CNN-LSTM-0.1	CNN-LSTM-0.2	Standard LSTM-0.1	Standard LSTM-0.2
	MAE(μg/s)	71.31	72	47.74	52.68	78.42	79.91
	R_{deg} (%)	-0.29	0.67	7.91	19.08	-0.52	1.37
	MRE(%)	11.47	11.72	6.24	6.68	11.31	11.48
Sensitivity deterioration	Model	Attention-LSTM-0.1	Attention-LSTM-0.2	CNN-LSTM-0.1	CNN-LSTM-0.2	Standard LSTM-0.1	Standard LSTM-0.2
	MAE(μg/s)	105.67	233.78	78.53	168.49	104.58	233.87
	R_{deg} (%)	47.75	226.87	77.51	280.85	32.67	196.68
	MRE(%)	16.2	29.07	9.81	16.6	16.21	27.44
Signal drift	Model	Attention-LSTM-0.2	Attention-LSTM-0.4	CNN-LSTM-0.2	CNN-LSTM-0.4	Standard LSTM-0.2	Standard LSTM-0.4
	MAE(μg/s)	361.73	598.28	238.38	375.6	352.24	543.78
	R_{deg} (%)	405.77	736.52	438.83	749.01	346.83	589.81
	MRE(%)	64.19	136.9	30.64	64.9	50.83	106.15

Sensitivity deterioration

Table 5 shows the models' predictions of MAE and MRE for sensitivity deterioration levels of 0.1 and 0.2. Sensor sensitivity decreases have a considerable detrimental influence on all models, and the degree of performance degradation is positively correlated with the sensitivity decline. Specifically, the CNN-LSTM model exhibits a sharp increase in error: its MAE rises from 78.53 μg/s at level 0.1 to 168.49 μg/s at level 0.2, accompanied by a drastic surge in the R_{deg} from 77.51% to 280.85%. Similarly, the Standard-LSTM shows significant vulnerability, with its MAE escalating from 104.58 μg/s to 233.87 μg/s and R_{deg} reaching 196.68% at level 0.2. Even the Attention-LSTM, despite its structural advantages, experiences its MAE more than doubling from 105.67 μg/s to 233.78 μg/s, resulting in an R_{deg} of 226.87%.

These systematic multiplicative errors are inherently difficult for the models to compensate for, as they induce scale deviations in predictions, thereby exacerbating the models' sensitivity to such degradation. Figure 6(e) depicts the timing diagram of the displacement signal for the CNN-LSTM model at the sensitivity reduction level of 0.1. While the model effectively captures the amplitude and phase variations of the flow during the initial prediction stage, the predicted amplitude gradually decays over time, leading to continuous error accumulation. Finally, a considerable scale deviation is formed in the later stages of prediction, resulting in a significant decrease in prediction accuracy.

Signal drift

Table 5 presents the MAE and MRE values of each model at sensor-drift levels of 0.2 and 0.4. In this condition, the prediction performance of all models has declined. The CNN-LSTM model exhibits extreme sensitivity to drift: its MAE surges from 238.38 μg/s at level 0.2 to 375.6 μg/s at level 0.4, with R_{deg} surging from 438.83% to 749.01%. Similarly, the Attention-LSTM's MAE climbs drastically from 361.73 μg/s to 598.28 μg/s, representing a 65.4% increase in absolute error between the two levels, while its R_{deg} nearly doubles from 405.77% to 736.52%. This persistent additive error (drift) fundamentally disrupts the model's learned input-output mapping, making it unable to distinguish between real physical signals and drift-induced pseudo-changes, resulting in continuous and significant prediction bias. Signal drift is a fundamental vulnerability shared by all models in this investigation.

Figure 6 (f) depicts the CNN-LSTM model's timing diagram at sensor-drift level 0.2. Except for the initial stage, the model's prediction curves vary dramatically from the real flow as the sensors drifts. The model largely loses its ability to capture the flow's amplitude and phase fluctuations, and its predicted peaks become saturated at an approximately constant level, indicating that the prediction results at this point have lost their reference value.

3.3 Discussion

The CNN-LSTM model achieves the highest prediction accuracy in interference-free scenarios and demonstrates superior robustness against data missing. However, its robustness degrades significantly when processing noisy data. This is primarily because the convolutional layers are highly sensitive to high-frequency signals, making them prone to mistakenly extracting random noise as local features, which subsequently disrupts the subsequent temporal modeling. In contrast, although the Attention-LSTM model has a slightly lower baseline prediction accuracy than the CNN-LSTM, it exhibits the best robustness in noisy environments. This advantage is attributed to the dynamic weight allocation capability of the attention mechanism, which effectively identifies and suppresses noise interference. The prediction accuracy of the Standard LSTM is comparable to that of the Attention-LSTM, while its robustness against noise remains at an intermediate level.

The robustness evaluation reveals a distinct difference in how data-driven models handle random disturbances versus systematic errors. Theoretically, deep learning models rely on learning the statistical distribution of the training data. Random disturbances primarily encompass data missing and Gaussian noise. For data missing, forward fill plays a pivotal role by repairing the sequence to ensure temporal continuity, thereby preventing state disruptions in the recurrent networks. Similarly, additive disturbances such as Gaussian noise typically exhibit a zero-mean property. These fluctuations are often mitigated by the model's nonlinear mapping capacity of Standard LSTM or Attention-based LSTM models. In contrast, when confronted with systematic degradations such as sensor sensitivity deterioration and sensor drift, the prediction performance and robustness of all three models experience an abrupt decline. This is primarily because such degradations introduce systematic errors that are difficult to compensate for, fundamentally destroying the mapping relationships learned by the models.

4. Conclusion

This study investigates data-driven flow prediction for piezoelectric microflow-control devices operating at the μg/s scale. Using 70,000 sets of observed data, three deep-learning models were constructed, evaluated, and compared in terms of predictive accuracy and robustness under simulated sensor degradation scenarios. The key findings are as follows:

1) The CNN-LSTM architecture delivers the best overall performance. The CNN-LSTM model performed well in the baseline test, with a minimum MAE of 44.24 μg/s and MRE of 8.5%. Compared to the Standard LSTM (MAE: 78.830 μg/s) and the Attention-LSTM (MAE: 71.517 μg/s), the prediction accuracy improves by 43.8% and 38.1%, respectively.
2) The spool displacement is the key factor that impacts prediction accuracy. In the Attention-LSTM, removing displacement features significantly increased MAE from 71.52 μg/s to 273.66 μg/s, resulting in a 282% error increase. After removing the voltage feature, the MAE decreased from 71.52 to 44.11 μg/s. This suggests that in engineering applications, the displacement sensor's data quality should be ensured first. For Attention-LSTM and Standard LSTM, excluding the voltage feature improved or slightly improved the MAE.
3) Compared to the other two architectures, the CNN-LSTM model demonstrates superior robustness against data missing. Notably, even with 30% of the data missing, it achieves a slight negative R_{deg} of -0.97%, indicating exceptional resilience. However, its robustness degrades significantly when handling random noise. Under a noise level of 0.2, R_{deg} surges to 19.08%. In contrast, the Attention-LSTM model exhibits outstanding robustness against noise, maintaining a negligible R_{deg} of only 0.67%

under the same 0.2 noise level. The robustness of the Standard LSTM model against noise remains at an intermediate level between the CNN-LSTM and the Attention-LSTM. Nevertheless, when confronted with systematic degradations such as sensitivity deterioration and signal drift, all three models experience an abrupt decline in performance.

This study not only verifies the technical advantages of advanced deep-learning models in accurate microflow prediction but also reveals the performance boundaries and key vulnerabilities of different architectures through detailed comparative analysis. These findings provide a basis for future research on health monitoring, sensor fusion, and robust control of piezoelectric microflow systems, paving the way for intelligent health management, sensor information fusion strategies, and highly robust control algorithms in aerospace applications.

However, the current study has several limitations. First, the prediction models demonstrate a strong dependence on the spool displacement sensor, meaning that the overall reliability of the system is heavily reliant on the quality of displacement data. Second, the models need to be further validated under broader pressure and temperature conditions to ensure their robustness across a wider range of operating environments. Finally, to effectively address the identified vulnerability to systematic signal drift, future work should focus on integrating these prediction models with online calibration and fault diagnosis algorithms.

Acknowledgements
This work was supported by Open Fund Project of Advanced Space Propulsion Technology Laboratory of Beijing Institute of Control Engineering (LabASP-2024-13).

References

[1] Zhang J X, Tao W J, Lian X B, et al. Present situation and trend of drag-free technology for space gravitational wave detection. Journal of National University of Defense Technology. 2024,46(2):1-17.
[2] Ni W D. Current status and prospects of space gravitational wave detection. Science China Physics, Mechanics & Astronomy. 2024,1-62.
[3] Li Y, Liu X H, Wang X D, et al. Review and prospect on the large-range thrust throttling technology with extremely small thrust. Aerospace Control and Application. 2019,45(6):1-12+19.
[4] Yu D R, Niu X, Wang T B,et al. Research progress of micropropulsion technology for space gravitational wave detection missions. Acta Scientiarum Naturalium Universitatis Sunyatseni. 2021,60(Z1):194-212.
[5] Awan M S U D, Elahi H, Ali A, et al. Advancement of nano-based piezoelectric material with integration of artificial intelligence in aerospace. Materials Today Sustainability. 2026, 35.
[6] Khandelwal V, Siroha P, Barik S, et al. Impact of oxygen vacancy reduction on the dielectric, energy storage, and electrocaloric properties of annealed BCZT ceramic. Journal of Materials Chemistry C. 2025, 13: 10178-10193.
[7] Ogunleye R O, Rusnáková S, Javořík J, et al. Advanced Sensors and Sensing Systems for Structural Health Monitoring in Aerospace Composites. Advanced Engineering Materials. 2024, 26.
[8] Yu Z L, Wu Y, Fang Z Y,et al. Modeling and compensation of hysteresis in piezoelectric actuators. Heliyon.2020,6(5):e03999.
[9] Gu G Y, Zhu L M, Su C Y, et al. Modeling and Control of Piezo-Actuated Nanopositioning Stages: A Survey. IEEE Transactions on Automation Science and Engineering. 2015,13(1):313-332.
[10] Hochreiter S, Schmidhuber J. Long short-term memory[J]. Neural Computation, 1997, 9(8): 1735-1780.
[11] Lakshmi S, Krishnamoorthy A. Centralized transfer-learning LSTM with multi-head attention for interpretable multi-pollutant forecasting in Delhi’s winter smog episodes. Engineering Research Express. 2025, 7.
[12] Mathuna K T, Elizabeth Shanthi I. Advanced Sentiment Analysis in Health Care Using Hybrid Transformer with LSTM-Based Deep Learning: A Social Media Data Perspective. *International Journal of Intelligent Engineering and Systems*. 2025, 18: 229-240.
[13] Nguyen T P. AIoT fault diagnosis framework of firefighting pump maintenance using hybrid CNN-LSTM deep learning technique. *International Journal of Data Science and Analytics*. 2026,22.
[14] Sherstinsky A. Fundamentals of recurrent neural network (RNN) and long short-term memory (LSTM) network. *Physica D: Nonlinear Phenomena*.2020,404:132306.
[15] Moon J, Lim S, Kim J, et al. A Study on the Mechanical Resonance Frequency of a Piezo Element: Analysis of Resonance Characteristics and Frequency Estimation Using a Long Short-Term Memory Model. Applied Sciences (Switzerland). 2024, 14.
[16] Razavi H, Moelans N. Physics-informed GCN-LSTM framework for long-term forecasting of 2D and 3D microstructure evolution. NPJ Computational Materials. 2026, 12.
[17] Kondru J B, Obulesu Y P. Hyper-heuristic optimized Bi-LSTM approach for accurate state-of-charge estimation of Ternary and $LiFePO_4$ batteries. Energy Reports. 2026, 16.
[18] Angeletti F, Gasbarri P, Panella M, et al. Multi-Damage Detection in Composite Space Structures via Deep Learning. Sensors. 2023, 23.
[19] Liu Y, Zhou R, Huo M. Long short term memory network is capable of capturing complex hysteretic dynamics in piezoelectric actuators. *Electronics Letters*, 2019, 55(2): 80-82.
[20] Patil M S, Charuku B, Ren J. Long Short-term Memory Neural Network-based System Identification and Augmented Predictive Control of Piezoelectric Actuators for Precise Trajectory Tracking. *IFAC-PapersOnLine*. 2021, 54(20): 38-45.
[21] Baker H, Brown L, Parrott A. On the use of LSTM-based estimation components for tokamak gas actuator control. *Fusion Engineering and Design*. 2025, 215: 114932.
[22] Al-Inizi F, Płaczek M, Wróbel A, et al. The Modelling Of A Hysteresis Graph Of Piezoelectric Elements Using Deep Learning Bidirectional LSTM. International Journal of Modern Manufacturing Technologies. 2024, 16. 24-38.